Spin-echo small-angle neutron scattering for multiscale structure analysis of food materials

Bouwman, W.G.

DOI
10.1016/j.foostr.2021.100235

Publication date
2021

Document Version
Final published version

Published in
Food Structure

Food Structure 30 (2021) 100235

Contents lists available at ScienceDirect

Food Structure

journal homepage: www.elsevier.com/locate/foostr

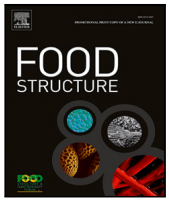

Spin-echo small-angle neutron scattering for multiscale structure analysis of food materials

Wim G. Bouwman

Delft University of Technology, Applied Sciences, Mekelweg 15, Delft, NL-2629 JB, The Netherlands

ARTICLE INFO

Keywords:
Small-angle neutron scattering
Food materials
Colloids
Protein networks
Emulsions

ABSTRACT

Spin-echo small-angle neutron scattering (SESANS) yields structural information on length scales from 30 nanometres up till 20 micrometres. These length scales match nicely those of colloids, protein networks and fat droplets, which are present in many food materials. This makes SESANS an excellent probe to study food materials. An interesting feature of SESANS is the real space character of the raw data. Several examples of quantitative neutron scattering studies on food materials are shortly reviewed.

1. Small-angle neutron scattering

The food industry seeks methods to produce high quality food with new, often more sustainable, ingredients. To rationally redesign food processing methods structural information on all length scales is needed. These length scales start from nanometres up to millimetres as illustrated in Fig. 1. In food, traditionally, macroscopic properties are measured, which do not yield directly structural information. Microscopic techniques give directly an easy to interpret image of the surface of a material, which for soft materials often is different from the structure of the bulk.

With scattering techniques it is possible to probe the bulk of statistically significant parts of a sample. Light scattering and X-ray scattering are widely available for this kind of analysis. Scattering yields quantitative descriptions of the structure of food that can be modelled based on input from microscopy. Neutron scattering is another natural probe to study food materials (Lopez-Rubio & Gilbert, 2009). Neutrons have the advantage that they can penetrate into the bulk of food materials and they are very sensitive for hydrogen. Neutrons penetrate easily through metals, which makes it feasible to develop a neutron transparent sample environment with realistic processing conditions, see for example (Doutch et al., 2012). By exchanging hydrogen by the chemically equivalent deuterium it is also possible to create a clear contrast, which makes it possible to label specific parts of a food system. Several examples are given in Gilbert (2019). In most of the examples given in this article a deuterated solvent is used to increase the scattered intensity, which further will be elaborated in the section on SESANS.

Several small-angle neutron scattering (SANS) techniques probe the length scales relevant for food as illustrated in Fig. 1. Conventional SANS probes length scales in the range of 1 - 300 nanometre (Gilbert, 2019; King, 1999). Spin-echo small angle neutron scattering (SESANS) (Rekveldt et al., 2005) and ultra small-angle neutron scattering (USANS) (Barker et al., 2005; Rehm et al., 2018) probe the longer length scales starting from 30 nanometre going up to 20 micrometres. It is relevant to be able to probe all these different length scales, since most food materials are hierarchical structures having different building blocks at each length scale. An interesting feature of SESANS is that the direct measurement data are in real space, which is for layman already interpretable without any strong background into scattering theory.

Some review articles on (small-angle) neutron scattering studies on food materials have been published (Gilbert, 2019; Lopez-Rubio & Gilbert, 2009). This paper reviews SESANS studies originating from the SESANS method developed at Delft University of Technology. First a short description of the SESANS method, data-analysis methods and instruments is given. Then studies are presented going from short length scales to longer length scales to illustrate the multiscale possibilities of the technique. First the aggregation of colloids and their interaction potential are studied. Then the quantitative characterisation of protein networks is presented. The article concludes with examples on larger structures, as fat droplets, air bubbles and fibre structures.

E-mail address: w.g.bouwman@tudelft.nl.

https://doi.org/10.1016/j.foostr.2021.100235
Received 20 May 2021; Received in revised form 24 September 2021; Accepted 29 September 2021
Available online 30 October 2021

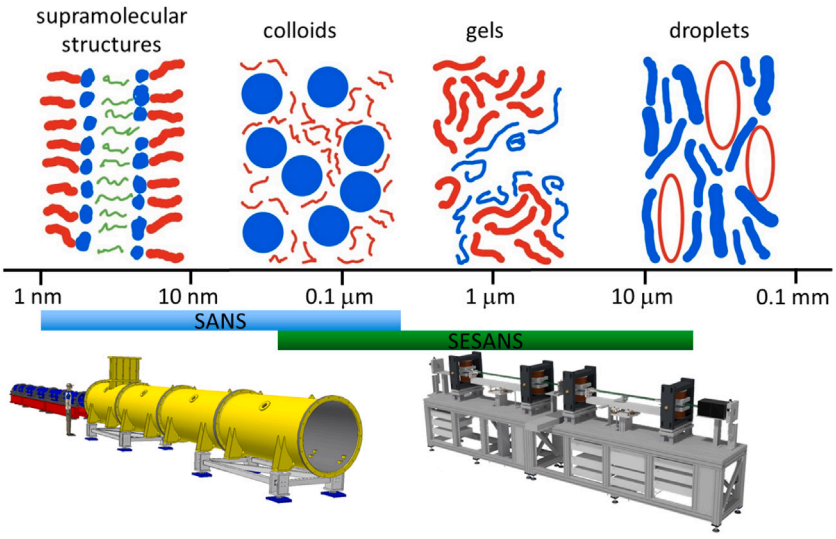

Fig. 1. Food materials can contain colloids, gels, droplets, fibres, air bubbles, etc. The related length scales range from nanometres up to millimetres. The shorter length scales can be probed with SANS and the longer length scales with SESANS and USANS.

2. Spin-echo small angle neutron scattering

2.1. Principle of SESANS

In conventional SANS the scattering cross section $I(Q)$ is measured as a function of the wave vector transfer Q. These measurements are performed by letting a collimated neutron beam hit a sample and then measuring the scattered neutrons on a position sensitive detector. There is large volume of literature on small-angle scattering models. There are several software packages available for data-analysis, such as SasFit (Breßler, Kohlbrecher, & Thünemann, 2015) and SasView (SasView) to help scientists to analyse their measurements.

In SESANS a polarised neutron beam is being used to measure the small-angle scattering. The Larmor precession of the neutron spin in magnetic fields is used to label the direction of the neutron path. Tilted interfaces between precession regions create this labelling, which can be achieved with several techniques. By using opposite senses of labelling before and after the sample a spin-echo is obtained for unscattered neutrons. Any small angle scattering will depolarise the neutron beam. The sensitivity for the scattering angle can be tuned with the applied magnetic field, the field geometry and the neutron wave length (Rekveldt et al., 2005). This tuning parameter is the so-called spin-echo length δ, which corresponds to the length scale probed in the sample. The polarisation that is measured as a function of spin-echo length can be calculated from the scattering cross section to be Bakker et al. (2020):

$$P(\delta) = e^{\lambda^2 t(G(\delta)-G(0))}, \tag{1}$$

in which λ is the neutron wavelength, t is the sample thickness and

$$G(\delta) = \frac{1}{2\pi}\int_0^\infty I(Q)J_0(Q\delta)QdQ, \tag{2}$$

in which J_0 is the zeroth order Bessel function of the first kind. The function $G(\delta)$ is the absolute scattering correlation function (Bakker et al., 2020), which is the 2D projection of the 3D auto-correlation function $\gamma(r)$ (Andersson, Van Heijkamp, De Schepper, & Bouwman, 2008; Kohlbrecher & Studer, 2017; Krouglov, De Schepper, Bouwman, & Rekveldt, 2003). This formulation of $G(\delta)$ is in absolute units, is independent on instrument and contains thus all information about the scattering characteristics of the sample. A direct representation of the experimental data, the polarisation $P(\delta)$ that allows for comparison between SESANS measurements performed at various SESANS instruments is by calculation of

$$\frac{\log(P(\delta))}{\lambda^2 t} = G(\delta) - G(0). \tag{3}$$

The unit cm^{-1} $Å^{-2}$ might look strange at first sight, however, the commonly used unit for sample thickness in neutron scattering is cm and the unit for neutron wavelength is Å. It is not possible to directly calculate $G(\delta)$, since it is from an experiment not directly possible to determine $G(0)$ without any experimental uncertainties. Some examples of calculated $G(\delta)-G(0)$ are shown in Fig. 2. The signal strength $G(0)$ is related to the scattering properties of the sample and can be calculated for a two-phase system to be (Andersson et al., 2008):

$$G(0) = (\Delta\rho)^2\phi(1-\phi)\xi, \tag{4}$$

in which $\Delta\rho$ represents the scattering length density contrast between the two phases, ϕ the volume fraction of one of the two phases and ξ the correlation length of the scattering length distribution (Andersson et al., 2008). The correlation length ξ is in practice roughly the most occurring distance in the density distribution, for example for a single sphere it is 0.75 times the diameter.

2.2. Data analysis

One convenient feature of SESANS compared to SANS is that the raw data are in real space, which makes data interpretation more intuitive. As an example four calculations of model systems are shown in Fig. 2. These calculations have been done in SasView (SasView). In all four examples a scattering length density contrast of $\Delta\rho = 6\times10^{-6}$ $Å^{-2}$ is used, which is a typical contrast between a normal organic material and a deuterated solvent.

- The first example, sphere, is a dilute dispersion of spheres with a diameter of 1 micrometre and a volume fraction $\phi = 0.03$. The signal shows a clear signal going down and saturating at a spin echo length equal to the diameter, which shows that at longer length scales the density correlation function does not change any longer. The signal strength can be read out directly in this case, since a clear saturation value of $G(0) = 0.81$ cm^{-1} $Å^{-2}$ is visible. This amplitude of the signal gives directly the information about the composition of the sample as represented in Eq. (4).
- The next calculation is performed on a concentrated dispersion of spheres with a diameter of 1 micrometre and a volume fraction $\phi = 0.25$ with a hard sphere interaction. One observes directly a peak at 1.2 micrometre, which corresponds to the nearest neighbour distance at this volume fraction. SESANS signals are directly sensitive to the interaction potential between colloids (Kruglov, Bouwman, de Schepper, & Rekveldt, 2005; Washington et al.,

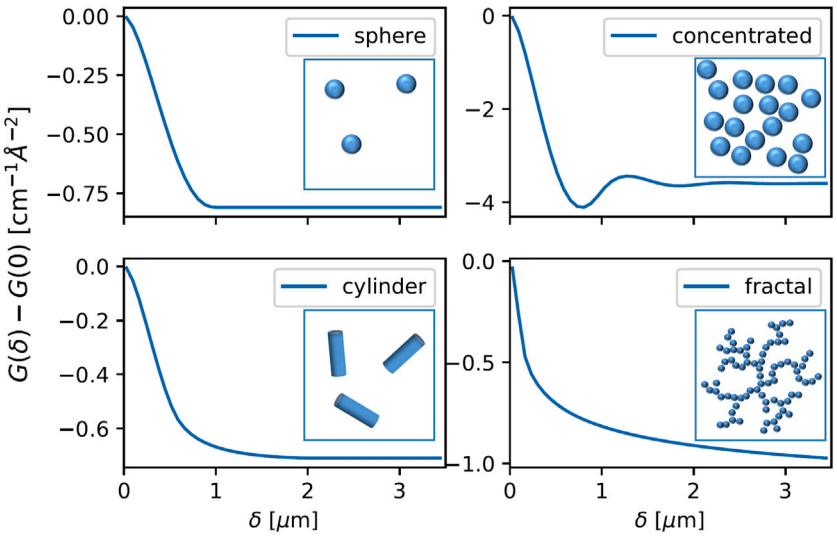

Fig. 2. Calculations of the signals $G(\delta) - G(0)$ for dilute spheres, concentrated spheres, cylinders and fractals using Eq. (2). Details of the calculation are given in the text. By visual interpretation some characteristics of the sample structure can be estimated, since the results are in real space instead of reciprocal space as is normally the case for scattering techniques.

2014). The value for $G(0)$ is larger than for the dilute case due to the higher volume fraction.

- The calculation for the cylinder is performed with a diameter of 0.6 micrometre, a length of 2 micrometre and a volume fraction $\phi = 0.03$. The diameter can be seen in the graph as the point where the signal nearly has reached saturation and where a low tail starts. The length of the cylinder is approximately where the signal really has reached its final value. The length is not a clear feature in SESANS.
- The fractal calculation represents a fractal-like aggregate of spheres with a diameter of 0.2 micrometre, a correlation length of 10 micrometre, a fractal dimension (Teixeira, 1988) with the value 1.8 and a volume fraction $\phi = 0.03$. The beginning of the calculation is very similar to the case for dilute spheres. At longer spin-echo length the aggregate becomes visible, however, since the correlation length is outside the view of the calculation, we do not observe a saturation of the signal. From the calculation we observe that the value of $G(0) > 1$ cm^{-1} Å^{-2} from which one can calculate via Eq. (4) that the correlation length $\xi > 1$ μm, which is larger than the radius of the elementary spheres and shorter than the fractal correlation length.

To do the full quantitative data-analysis some analytical forms for the absolute scattering correlation function are known (Andersson et al., 2008; Krouglov et al., 2003) and can be used directly to fit the data. Another option is to use the Hankel transform as described in Eq. (2) on known models from small-angle scattering. This second method has been implemented in the freely available packages SasView and SasFit (Breßler et al., 2015; SasView), which makes it possible to apply many different small-angle scattering models.

2.3. Instrumentation

The first dedicated SESANS instrument was installed at reactor of the Delft University of Technology (Rekveldt et al., 2005). This instrument is using a fixed wavelength, which makes it possible to use thin foil polarisation flippers to define the precession regions with a sharp angle, yielding a maximum spin-echo length of 20 μm even though only thermal neutrons with a wavelength of 2 Å are used. Typical data acquisition times for a single measurement are one hour. The examples cited in this article are all measured at this instrument.

At the spallation source ISIS there are spin-echo components installed at the instrument Larmor, which makes it possible to do SANS measurements, SESANS measurements and both simultaneously (Schmitt et al., 2020). RF-flippers with tilted magnetic interfaces create the precession gradient for a wide wavelength band (Plomp, De Haan, Dalgliesh, Langridge and van Well, 2007). This shows the advantage of presenting the data as $\log(P(\delta)/(\lambda^2 t))$ instead of $P(\delta)$ to make it possible to compare measurements with different instrument settings. Due to the long wavelengths available in the instrument spin-echo length of 20 μm can be reached.

As an add-on used at neutron instruments are Wollaston prisms (Li et al., 2016, 2014) used to perform SESANS measurements. Wollaston prisms are triangular shaped magnetic fields defined with superconducting foils. This is the most basic manner to create a gradient in precession to label the direction of the neutron path without any wavelength dependent neutron spin manipulation devices. These Wollaston prisms have thus the advantage that they work in a wide wavelength range. A dedicated instrument with Wollaston prisms is installed at the LENS facility at Indiana University (Parnell et al., 2015). The related technique SEMSANS (Bouwman, Duif, Plomp, Wiedenmann, & Gähler, 2011) using the Wollaston prisms is available on the HFIR instrument suite in Oak Ridge (Dadisman et al., 2019).

A dedicated instrument is being built in the PIK reactor in Gatchina using RF-flippers (Kraan et al., 2014).

Several neutron resonance spin-echo spectrometers are installed in for example the FRM2 in Munich and the ILL in Grenoble, where in principle the instrument could be used for SESANS measurements as was shown in the first SESANS experiment (Keller, Gähler, Kunze, & Golub, 1995). However, these instruments are not optimised for SESANS measurements.

2.4. Comparison with SANS and USAns

The functional main difference between SANS and SESANS are the length scales at which the techniques are sensitive. SANS can measure at shorter length scales than SESANS as depicted in Fig. 1. The results from SANS are in reciprocal space, which makes the measurement data less intuitive to interpret. SANS measures the complete 2D scattering pattern, so for anisotropically scattering samples SANS is much more convenient.

USANS is a related technique sensitive at the same length scales as SESANS (Barker et al., 2005; Rehm et al., 2018). These instruments are basically two-crystal diffractometers with a very high resolution in only one direction, which is the same in SESANS. However, the

results are in reciprocal space, just like in conventional SANS. The performance of SESANS and USANS are broadly rather similar (Rehm, Barker, Bouwman, & Pynn, 2013). USANS performs better for weakly scattering samples and SESANS for stronger scattering samples. The data-acquisition times are also typically one hour. USANS instruments are also used for food science in a similar way as SESANS, for example to study casein micelles (De Kruif, Huppertz, Urban, & Petukhov, 2012; Peyronel, Marangoni, & Pink, 2020; Smith, Brok, Christiansen, & Ahrné, 2020).

3. Colloids

One of the main constituents of fat-free milk are the casein micelles. Milk and other dairy products are difficult to study with conventional light scattering, since they are optically dense. With microscopic techniques with greater or lesser preparation of the sample it is possible to get a good image of a dairy product. The scattering methods have the advantage that the micelles can be studied in conditions approximating to their native state (Dalgleish, 2014). With SESANS (Tromp & Bouwman, 2007) the size distribution around some 100 nm of the micelles has been confirmed as measured by other techniques. The signal is very comparable to the sphere calculation in Fig. 2, however convolved with a size distribution. By curdling one can make cheese from milk and by acidification one can make yoghurt with length scales up to some 5 μm. These gels are similar to the fractal-like case in Fig. 2. The yoghurt gel is slightly less dense than the initial cheese curd (Tromp & Bouwman, 2007). By careful analysis of the density correlation function obtained by SESANS and USANS it is possible to quantify the yoghurt gels. By comparing the structures and kinetic USANS measurements the aggregation model has been determined (van Heijkamp et al., 2010). The measurements were best described by starting with reaction limited cluster–cluster aggregation and ending with diffusion limited cluster–cluster aggregation. Recently, USANS measurements have been published on aggregates of both skimmed and whole milk that show that the fractal structure depends on the rennet used (Callaghan-Patrachar, Peyronel, Pink, Marangoni, & Adams, 2021). One point of concern is the potential effect of using D_2O as a solvent to increase contrast on the aggregation behaviour. It is known that deuterated solvent can effect biological processes.

Colloidal gels are applied in many food applications. The interaction potential between the colloidal particles can be fine tuned by Coulomb repulsion and polymer depletion interaction (van Gruijthuijsen, Bouwman, Schurtenberger, & Stradner, 2014; Van Gruijthuijsen, Obiols-Rabasa, Schurtenberger, Bouwman, & Stradner, 2018). By adding salt to charged colloids in water, the Coulomb repulsion can be screened. By adding polymers the depletion attraction is increased. This gives controls to fine tune the repulsive and attractive components in the interaction potential. The measurements have features in common with the concentrated case in Fig. 2 for the samples without polymer. With enough polymer added the measurements look more like the fractal-like aggregates. With a combination of SAXS and SESANS measurement the interaction potential as a function of composition is completely quantified (Van Gruijthuijsen et al., 2018). This makes it possible to prepare new gels with desired properties.

4. Networks

Water holding capacity is an important property of food materials: it determines the juiciness and the release of tastants during eating. Understanding the relation between structure and water holding is crucial for texture design of food materials. SESANS measurements were performed on ovalbumin gels prepared at different acidities (Nieuwland, Bouwman, Pouvreau, Martin, & de Jongh, 2016). The SESANS measurements could be described with a two-level structure, the finer one with a radius of some 0.2 μm and the larger with a radius of some 7 μm, just as if one would add to sphere curves with a very different radius from Fig. 2. The more open aggregates turned out to have a higher water holding capacity (Nieuwland et al., 2016).

Gels are formed when molecules, typically proteins or polysaccharides, associate into a large network, reducing the mobility of the solvent. Only small concentrations of gel molecules are enough to observe a transition from a liquid into a solid-like state. Two gelating biopolymers together might influence each other's gelation behaviour. The gelation of globular proteins in the presence of small concentrations of gelatin was studied with SESANS (Ersch et al., 2016). The final gel structures can all be described with a fractal-like model, the self-affine random density distribution model. The relevant length scales in the gels were between 100 and 1000 nm. The addition of the gelatin led to a courser gel structure. The mechanism could be that the gelatin leads in the initial stage of gelation to a phase separation between the protein rich and gelatin rich phase. This helps to understand how to fine tune the properties of the final gel structure.

5. Droplets and fibres

Many food materials, as for example fresh cheese products, are optically opaque emulsion gels. Properties like firmness and syneresis of emulsion gels are determined by the structural organisation of the emulsion droplet clusters (Bot, Duval, Duif and Bouwman, 2007). The effect of processing on the droplet cluster structure of emulsion gels stabilised with whey protein-stabilised oil-in-water emulsion gels was studied by SESANS (Bot, Duval and Bouwman, 2007). The correlation function of the oil density distribution function was determined after several processing methods. The correlation length describing the density distribution was varying from 2 to 10 μm. The structure is more affected by temperature cycling and acidification than by the number of homogenisation steps. This helps to further optimise the production process of these food products.

Texture is crucial for the acceptance by the consumer of meat analogues (Tian et al., 2019). The fibre density and their alignment in meat analogues made by shearing soy protein isolate and gluten was measured by SESANS (Krintiras et al., 2014). Air bubbles seem to be relevant for the formation of fibres in meat analogues (Tian, Wang, van der Goot, & Bouwman, 2018). Both fibres and air bubbles can be relatively large, with relevant length scales larger than some 50 micrometre. At these length scales the formalism of scattering is not applicable any longer since the neutrons can undergo a phase shift while going through an object. In that case the change in angle has to be described with geometrical optics as has been shown for metal wires (Plomp, Barker, De Haan, Bouwman and van Well, 2007). These measurements can give information on the number of refracting objects and the orientation of the refracting interfaces. In the case of the fibre study, the refraction determined the number of fibres and their respective orientation (Krintiras et al., 2014). With the air bubble study the bubbles where modelled as sphero-cylinders, where their length/diameter ratio and their number density were measured (Tian et al., 2018). The results were confirmed with X-ray tomography. At present this information is ex-situ more quantitatively available with microscopy or X-ray tomography. However, the final aim of these measurement is to do these measurements under processing conditions to monitor what is really happening.

6. Conclusions and outlook

In the examples given above the length scales were ranging over three orders in magnitude. All examples were based on multidisciplinary collaboration between neutron scattering and food scientists. It is important to note that neutron scattering was in all these studies only one of the many tools to characterise the food materials. Quite often the neutron scattering experiment was the last measurement to really quantify a structure of which many other properties where already

known to some extent. This made it possible to describe the scattering data with sensible models.

The data analysis was one of the main obstacles to overcome in these experiments. Many model descriptions in neutron scattering are developed for well defined, monodisperse 2-component systems. Food, in contrast, is inherently inhomogeneous, polydisperse and polymorphic which is not incorporated in the normally used models. So new models have to be developed to continue with further food scattering experiments. For example, with polydisperse systems a length scale can be determined with the right model (Tian, Heringa, & Bouwman, 2021). This length scale can then be determined as a function of the processing parameters to study their effect on the structure (Tian et al., 2020).

A real challenge will be to develop and build more sample environments to measure in-situ under realistic processing conditions (Doutch et al., 2012; Velichko et al., 2019).

Declaration of competing interest

The authors declare that they have no known competing financial interests or personal relationships that could have appeared to influence the work reported in this paper.

Acknowledgements

I thank all the co-authors of the cited neutron scattering papers for the interesting complementary collaboration. I am specially grateful to all the Ph.D. students who did the hard work of sample preparations and most of the measurements. It is a great pleasure to work in these multidisciplinary projects with food scientists.

This work benefited from the use of the SasView application, originally developed under NSF award DMR-0520547. SasView contains code developed with funding from the European Union's Horizon 2020 research and innovation programme under the SINE2020 project, grant agreement No 654000. All of the reviewed studies are financed by the Netherlands Organisation for Scientific Research (NWO). The details can be found in the original papers.

The author thanks the participants of the workshop on Multiscale simulations and experimental Analysis of Food, Wageningen (Bouwman, 2021) for their useful comments. The author thanks Dr. Steven Parnell for critical reading of the manuscript. The author thanks also the reviewers for their constructive comments that have greatly improved this paper.

References

Andersson, R., Van Heijkamp, L. F., De Schepper, I. M., & Bouwman, W. G. (2008). Analysis of spin-echo small-angle neutron scattering measurements. *Journal of Applied Crystallography*, *41*(5), 868–885.

Bakker, J. H., Washington, A. L., Parnell, S. R., Van Well, A. A., Pappas, C., & Bouwman, W. G. (2020). Analysis of SESANS data by numerical Hankel transform implementation in SasView. *Journal of Neutron Research*, *22*(1), 57–70.

Barker, J., Glinka, C., Moyer, J., Kim, M., Drews, A., & Agamalian, M. (2005). Design and performance of a thermal-neutron double-crystal diffractometer for USAns at NIST. *Journal of Applied Crystallography*, *38*(6), 1004–1011.

Bot, A., Duval, F. P., & Bouwman, W. G. (2007). Effect of processing on droplet cluster structure in emulsion gels. *Food Hydrocolloids*, *21*(5–6), 844–854.

Bot, A., Duval, F. P., Duif, C. P., & Bouwman, W. G. (2007). Probing the droplet cluster structure in acidified temperature-cycled o/w emulsion gels by means of SESANS. *International Journal of Food Science & Technology*, *42*(6), 746–752.

Bouwman, W. G. (2021). Multi scale structure analysis of food materials with scattering. In *Workshop multiscale simulations and experimental analysis of food, Wageningen 25-27 May 2021*. URL http://dx.doi.org/10.5281/zenodo.5068030.

Bouwman, W. G., Duif, C. P., Plomp, J., Wiedenmann, A., & Gähler, R. (2011). Combined SANS–SESANS, from 1 nm to 0.1 mm in one instrument. *Physica B: Condensed Matter*, *406*(12), 2357–2360.

Breßler, I., Kohlbrecher, J., & Thünemann, A. F. (2015). Sasfit: a tool for small-angle scattering data analysis using a library of analytical expressions. *Journal of Applied Crystallography*, *48*(5), 1587–1598.

Callaghan-Patrachar, N., Peyronel, F., Pink, D., Marangoni, A., & Adams, C. (2021). USANs and SANS investigations on the coagulation of commercial bovine milk: Microstructures induced by calf and fungal rennet. *Food Hydrocolloids*, *116*, Article 106622.

Dadisman, R., Shen, J., Feng, H., Crow, L., Jiang, C., Wang, T., et al. (2019). Design and characterization of zero magnetic field chambers for high efficiency neutron polarization transport. *Nuclear Instruments and Methods in Physics Research Section A: Accelerators, Spectrometers, Detectors and Associated Equipment*, *940*, 174–180.

Dalgleish, D. G. (2014). The basis of structure in dairy-based foods: Casein micelles and their properties. In *Food structures, digestion and health* (pp. 83–105). Elsevier.

De Kruif, C. G., Huppertz, T., Urban, V. S., & Petukhov, A. V. (2012). Casein micelles and their internal structure. *Advances in Colloid and Interface Science*, *171*, 36–52.

Doutch, J., Bason, M., Franceschini, F., James, K., Clowes, D., & Gilbert, E. P. (2012). Structural changes during starch pasting using simultaneous rapid visco analysis and small-angle neutron scattering. *Carbohydrate Polymers*, *88*(3), 1061–1071.

Ersch, C., Meinders, M. B., Bouwman, W. G., Nieuwland, M., van der Linden, E., Venema, P., et al. (2016). Microstructure and rheology of globular protein gels in the presence of gelatin. *Food Hydrocolloids*, *55*, 34–46.

Gilbert, E. P. (2019). Small-angle X-Ray and neutron scattering in food colloids. *Current Opinion in Colloid & Interface Science*, *42*, 55–72.

van Gruijthuijsen, K., Bouwman, W. G., Schurtenberger, P., & Stradner, A. (2014). Direct comparison of SESANS and SAXS to measure colloidal interactions. *EPL (Europhysics Letters)*, *106*(2), 28002.

van Heijkamp, L. F., de Schepper, I. M., Strobl, M., Tromp, R. H., Heringa, J. R., & Bouwman, W. G. (2010). Milk gelation studied with small angle neutron scattering techniques and Monte Carlo simulations. *The Journal of Physical Chemistry A*, *114*(7), 2412–2426.

Keller, T., Gähler, R., Kunze, H., & Golub, R. (1995). Features and performance of an NRSE spectrometer at BENSC. *Neutron News*, *6*(3), 16–17.

King, S. M. (1999). Small-angle neutron scattering. *Modern Techniques for Polymer Characterisation*, *12*.

Kohlbrecher, J., & Studer, A. (2017). Transformation cycle between the spherically symmetric correlation function, projected correlation function and differential cross section as implemented in sasfit. *Journal of Applied Crystallography*, *50*(5), 1395–1403.

Kraan, W., Akselrod, L., Chetverikov, Y. O., Grigoriev, S., Moskwin, E., Piyadov, V., et al. (2014). Present status and prospects for spin-echo small-angle neutron scattering (SESANS) at PIK neutron source. *Journal of Surface Investigation. X-Ray, Synchrotron and Neutron Techniques*, *8*(5), 1035–1043.

Krintiras, G. A., Göbel, J., Bouwman, W. G., Van Der Goot, A. J., & Stefanidis, G. D. (2014). On characterization of anisotropic plant protein structures. *Food & Function*, *5*(12), 3233–3240.

Krouglov, T., De Schepper, I. M., Bouwman, W. G., & Rekveldt, M. T. (2003). Real-space interpretation of spin-echo small-angle neutron scattering. *Journal of Applied Crystallography*, *36*(1), 117–124.

Kruglov, T. V., Bouwman, W. G., de Schepper, I. M., & Rekveldt, T. M. (2005). Application of spin-echo small-angle neutron scattering to study the structure of charged colloids. *Physica B: Condensed Matter*, *356*(1–4), 218–222.

Li, F., Parnell, S. R., Bai, H., Yang, W., Hamilton, W. A., Maranville, B. B., et al. (2016). Spin echo modulated small-angle neutron scattering using superconducting magnetic wollaston prisms. *Journal of Applied Crystallography*, *49*(1), 55–63.

Li, F., Parnell, S., Hamilton, W., Maranville, B., Wang, T., Semerad, R., et al. (2014). Superconducting magnetic wollaston prism for neutron spin encoding. *Review of Scientific Instruments*, *85*(5), Article 053303.

Lopez-Rubio, A., & Gilbert, E. P. (2009). Neutron scattering: a natural tool for food science and technology research. *Trends in Food Science & Technology*, *20*(11–12), 576–586.

Nieuwland, M., Bouwman, W. G., Pouvreau, L., Martin, A. H., & de Jongh, H. H. (2016). Relating water holding of ovalbumin gels to aggregate structure. *Food Hydrocolloids*, *52*, 87–94.

Parnell, S., Washington, A., Li, K., Yan, H., Stonaha, P., Li, F., et al. (2015). Spin echo small angle neutron scattering using a continuously pumped 3he neutron polarisation analyser. *Review of Scientific Instruments*, *86*(2), Article 023902.

Peyronel, F., Marangoni, A. G., & Pink, D. A. (2020). Using the USAxs technique to reveal the fat globule and casein micelle structures of bovine dairy products. *Food Research International*, *129*, Article 108846.

Plomp, J., Barker, J., De Haan, V., Bouwman, W., & van Well, A. (2007). Neutron refraction by cylindrical metal wires. *Nuclear Instruments and Methods in Physics Research Section A: Accelerators, Spectrometers, Detectors and Associated Equipment*, *574*(2), 324–329.

Plomp, J., De Haan, V., Dalgliesh, R., Langridge, S., & van Well, A. (2007). Neutron spin-echo labelling at OffSpec, an ISIS second target station project. *Thin Solid Films*, *515*(14), 5732–5735.

Rehm, C., Barker, J., Bouwman, W. G., & Pynn, R. (2013). Dcd usans and sesans: a comparison of two neutron scattering techniques applicable for the study of large-scale structures. *Journal of Applied Crystallography*, *46*(2), 354–364.

Rehm, C., Campo, L. d., Brûlé, A., Darmann, F., Bartsch, F., & Berry, A. (2018). Design and performance of the variable-wavelength bonse–hart ultra-small-angle neutron scattering diffractometer kookaburra at ANSTO. *Journal of Applied Crystallography*, *51*(1), 1–8.

Rekveldt, M. T., Plomp, J., Bouwman, W. G., Kraan, W. H., Grigoriev, S., & Blaauw, M. (2005). Spin-echo small angle neutron scattering in delft. *Review of Scientific Instruments*, *76*(3), Article 033901.

SasView. Sasview for Small Angle Scattering Analysis, https://www.sasview.org/.

Schmitt, J., Zeeuw, J. J., Plomp, J., Bouwman, W. G., Washington, A. L., Dalgliesh, R. M., et al. (2020). Mesoporous silica formation mechanisms probed using combined spin–echo modulated small-angle neutron scattering (SEMSANS) and small-angle neutron scattering (SANS). *ACS Applied Materials & Interfaces*, *12*(25), 28461–28473.

Smith, G. N., Brok, E., Christiansen, M. V., & Ahrné, L. (2020). Casein micelles in milk as sticky spheres. *Soft Matter*, *16*(43), 9955–9963.

Teixeira, J. (1988). Small-angle scattering by fractal systems. *Journal of Applied Crystallography*, *21*(6), 781–785.

Tian, B., Heringa, J., & Bouwman, W. G. (2021). Scattering from oriented objects analysed by the anisotropic guinier-porod model. *Food Structure*, *30*, Article 100221.

Tian, B., Sakai, V. G., Pappas, C., van der Goot, A. J., & Bouwman, W. G. (2019). Fibre formation in calcium caseinate influenced by solvent isotope effect and drying method–a neutron spectroscopy study. *Chemical Engineering Science*, *207*, 1270–1277.

Tian, B., Wang, Z., de Campo, L., Gilbert, E. P., Dalgliesh, R. M., Velichko, E., et al. (2020). Small angle neutron scattering quantifies the hierarchical structure in fibrous calcium caseinate. *Food Hydrocolloids*, *106*, Article 105912.

Tian, B., Wang, Z., van der Goot, A. J., & Bouwman, W. G. (2018). Air bubbles in fibrous caseinate gels investigated by neutron refraction, X-ray tomography and refractive microscope. *Food Hydrocolloids*, *83*, 287–295.

Tromp, R. H., & Bouwman, W. G. (2007). A novel application of neutron scattering on dairy products. *Food Hydrocolloids*, *21*(2), 154–158.

Van Gruijthuijsen, K., Obiols-Rabasa, M., Schurtenberger, P., Bouwman, W., & Stradner, A. (2018). The extended law of corresponding states when attractions meet repulsions. *Soft Matter*, *14*(19), 3704–3715.

Velichko, E., Tian, B., Nikolaeva, T., Koning, J., van Duynhoven, J., & Bouwman, W. G. (2019). A versatile shear cell for investigation of structure of food materials under shear. *Colloids and Surfaces A: Physicochemical and Engineering Aspects*, *566*, 21–28.

Washington, A., Li, X., Schofield, A. B., Hong, K., Fitzsimmons, M., Dalgliesh, R., et al. (2014). Inter-particle correlations in a hard-sphere colloidal suspension with polymer additives investigated by spin echo small angle neutron scattering (SESANS). *Soft Matter*, *10*(17), 3016–3026.